Annales Geophysicae

Revising the retrieval technique of a long-term stratospheric HNO$_3$ data set: from a constrained matrix inversion to the optimal estimation algorithm

I. Fiorucci[1], G. Muscari[1], and R. L. de Zafra[2]

[1]Istituto Nazionale di Geofisica e Vulcanologia, Rome, Italy
[2]Department of Physics and Astronomy, State University of New York at Stony Brook, Stony Brook, NY, USA

Abstract. The Ground-Based Millimeter-wave Spectrometer (GBMS) was designed and built at the State University of New York at Stony Brook in the early 1990s and since then has carried out many measurement campaigns of stratospheric O$_3$, HNO$_3$, CO and N$_2$O at polar and mid-latitudes. Its HNO$_3$ data set shed light on HNO$_3$ annual cycles over the Antarctic continent and contributed to the validation of both generations of the satellite-based JPL Microwave Limb Sounder (MLS). Following the increasing need for long-term data sets of stratospheric constituents, we resolved to establish a long-term GMBS observation site at the Arctic station of Thule (76.5° N, 68.8° W), Greenland, beginning in January 2009, in order to track the long- and short-term interactions between the changing climate and the seasonal processes tied to the ozone depletion phenomenon. Furthermore, we updated the retrieval algorithm adapting the Optimal Estimation (OE) method to GBMS spectral data in order to conform to the standard of the Network for the Detection of Atmospheric Composition Change (NDACC) microwave group, and to provide our retrievals with a set of averaging kernels that allow more straightforward comparisons with other data sets. The new OE algorithm was applied to GBMS HNO$_3$ data sets from 1993 South Pole observations to date, in order to produce HNO$_3$ version 2 (v2) profiles. A sample of results obtained at Antarctic latitudes in fall and winter and at mid-latitudes is shown here. In most conditions, v2 inversions show a sensitivity (i.e., sum of column elements of the averaging kernel matrix) of 100 ± 20 % from 20 to 45 km altitude, with somewhat worse (better) sensitivity in the Antarctic winter lower (upper) stratosphere. The 1σ uncertainty on HNO$_3$ v2 mixing ratio vertical profiles depends on altitude and is estimated at $\sim$15 % or 0.3 ppbv, whichever is larger. Comparisons of v2 with former (v1) GBMS HNO$_3$ vertical profiles, obtained employing the constrained matrix inversion method, show that v1 and v2 profiles are overall consistent. The main difference is at the HNO$_3$ mixing ratio maximum in the 20–25 km altitude range, which is smaller in v2 than v1 profiles by up to 2 ppbv at mid-latitudes and during the Antarctic fall. This difference suggests a better agreement of GBMS HNO$_3$ v2 profiles with both UARS/ and EOS Aura/MLS HNO$_3$ data than previous v1 profiles.

Keywords. Atmospheric composition and structure (Instruments and techniques)

1 Introduction

Nitric Acid (HNO$_3$) is a major player in processes controlling the springtime depletion of polar ozone, both over short and long time periods. It is a primary reservoir for reactive nitrogen in the stratosphere and has a key role in both the activation and the deactivation of chlorine species (Brasseur and Solomon, 1984). HNO$_3$ is the main constituent of Polar Stratospheric Cloud (PSC) particles, which develop in the extremely low temperatures observed in polar winters. PSC particles provide surfaces for heterogeneous reactions through which chlorine is converted from its reservoir species (e.g., ClONO$_2$, HCl) to highly reactive forms (e.g., ClO) that participate in springtime ozone-depleting processes (Solomon et al., 1986). Additionally, the sequestration of HNO$_3$ in PSC particles and the subsequent gravitational settling permanently remove a significant amount of active nitrogen from the stratosphere in a process known as denitrification (e.g., Fahey et al., 1989). After the return of warmer temperatures in spring, HNO$_3$ incorporated

into PSC aerosols which have not settled out of the stratosphere returns in the gas phase and is photolized, releasing NO$_2$ promoting the chlorine deactivation via the reformation of ClONO$_2$. Denitrification therefore delays the deactivation of chlorine and leads to prolonged ozone loss during polar spring (e.g., Tabazadeh et al., 2000, 2001).

As a result of international regulations controlling the production of ozone-depleting substances, the ozone layer is expected to recover back to 1980 levels in the next 60 years (Newman et al., 2006). However potential changes in Earth's climate, driven by rising concentrations of greenhouse gases, may have a strong impact on this expected recovery (WMO, 2007). Variations in the stratospheric circulation and temperature, leading to possible cooling and moistening, may alter the occurrence and duration of PSCs activity, influencing the future ozone levels significantly. Monitoring HNO$_3$ and its long-term variability, especially in polar regions, can therefore contribute to better understand the interdependence between a changing climate and the recovery of the stratospheric ozone layer.

Starting in 1993, HNO$_3$ observations have been carried out by means of a Ground-Based Millimeter-wave Spectrometer (GBMS) from a variety of sites in both hemispheres, at polar and mid-latitudes (de Zafra et al., 1997; Muscari et al., 2007; Santee et al., 2007). In Antarctica, GBMS HNO$_3$ measurements were obtained from the Amundsen Scott Base at the South Pole during the greater part of 1993, 1995 (McDonald et al., 2000), and 1999. These measurements represent a unique data record of stratospheric nitric acid profiles quasi-continuously covering full year cycles in the Antarctic region. From February 2004 to March 2007 several GBMS field campaigns, mostly during winter and fall, were carried out from the Alpine site of Testa Grigia (45.9° N, 7.7° E, elev. 3500 m), at the border between Italy and Switzerland. GBMS HNO$_3$ data sets from both polar and mid-latitude sites were compared to satellite measurements, first with UARS/MLS (Muscari et al., 2002) and later with Aura/MLS (Santee et al., 2007). In January 2009 the GBMS was moved to the NDACC (Network for the Detection of Atmospheric Composition Change) polar station at Thule (76.5° N, 68.8° W), Greenland, where it has been operated, mostly on a daily basis, from January to March 2009 (Di Biagio et al., 2010), 2010 (Fiorucci et al., 2009), and 2011. Regular winter measurement campaigns are planned in the future.

Until recently, GBMS HNO$_3$ spectra were deconvolved to produce stratospheric HNO$_3$ mixing ratio vertical profiles using an algorithm known as constrained matrix inversion (MI) (Twomey, 1977; de Zafra et al., 1997). Although this technique has its advantages versus other more popular algorithms (e.g., the solution profile is basically independent of the "a priori" concentration profile), profiles retrieved using the MI algorithm cannot be easily compared to other data sets due to the lengthy process required for determining their corresponding averaging kernels (AKs), AKs being necessary to reduce the reference data sets to the typically lower vertical resolution of the GBMS data.

In view of a growing need for long-term data sets for both monitoring middle atmospheric chemical compounds and validating shorter-term satellite-based measurements, the full GBMS data set is being reanalyzed adapting the Optimal Estimation (OE) method (Rodgers, 1976, 2000; Nedoluha et al., 1995) to the GBMS spectral measurements of O$_3$, CO, HNO$_3$, and N$_2$O. Moreover, it is desirable that both past and future GBMS data submissions to the NDACC data base should be derived using a standard spectral deconvolution technique which provides a set of AKs univocally defined in the frame of the NDACC.

In this paper we describe the adaptation of the OE general theory to GBMS HNO$_3$ spectra. The drastic changes in HNO$_3$ spectral features due to GBMS different observing sites and seasons, made clear the importance and subtlety of OE parameter selection and tuning. We emphasize this aspect here, illustrating capabilities and limitations of the OE technique applied to GBMS HNO$_3$ spectra. We also compare the new HNO$_3$ vertical profiles (hereafter referred to as version 2 or v2) to those obtained in the past using the constrained matrix inversion method (hereafter referred to as version 1 or v1) to evaluate how the change in retrieval algorithm might affect previous comparisons carried out using the GBMS MI-based HNO$_3$ retrievals.

2 GBMS observing technique

The GBMS was originally designed and built at the Physics and Astronomy Department of the State University of New York at Stony Brook in the late 1980s (de Zafra, 1995; Parrish et al., 1988), with periodic technical upgrades since then. In its present form, it consists of a high-sensitivity heterodyne receiver employing a superconducting SIS junction, followed by a back-end spectrometer. The heterodyne receiver converts millimeter-wave signals (230–280 GHz range) arising from molecular rotational transitions to the lower Intermediate Frequency (IF) of 1.4 GHz. The IF output contains all the spectral information of the incoming signal but is shifted to much lower frequencies where it can be amplified. This output is then sent to the backend spectrometer (initially consisting of filter banks, later replaced by an Acousto-Optical Spectrometer (AOS)), which produces the intensity vs. frequency spectrum that is analyzed to retrieve a vertical distribution. Both the filter banks and the AOS have 512 read-out channels, with a resolution of 1 MHz and 1.2 MHz, respectively. The GBMS frequency window of 512 MHz (for filter banks) or 600 MHz (using the AOS) can be tuned between 230 and 280 GHz. Taking advantage of the dependence of the emission line broadening on atmospheric pressure, deconvolution algorithms allow the retrieval of mixing ratio vertical profiles for the observed trace gases. Assuming a generic line pressure broadening of about

3 MHz/mb, the GBMS bandwidth and resolution limit the altitude range where the trace gases concentration can be retrieved from ∼15 to ∼50 km.

During normal data taking operations the GBMS observes radiation from two different directions 75° to 80° apart (signal and reference beams), switched by a rotating reflective semicircular chopper wheel at ∼1 Hz frequency. A dielectric sheet (made of Plexiglas) mounted in the reference beam acts as a local partially transparent (and weakly emitting) "grey body" source of broad-band radiation to compensate for the lower total power received from atmospheric emission near the zenith (with a shorter geometrical path length with respect to the signal beam), and allows a power balance to be achieved between the two directions. As atmospheric opacity increases or decreases (causing thermal emission from the atmosphere to increase or decrease), a servo mechanism, seeking to maintain power balance in the two beams, will drive the signal beam angle upwards or downwards. Atmospheric radiation from both beam directions enters through a window made of type PP-2 Eccofoam characterized by a very small opacity at millimeter wavelengths (∼0.007 Nepers). Further information on the GBMS observing technique and involved equations can also be found in the recent work by Fiorucci et al. (2008).

The HNO₃ spectrum observed by the GBMS is rather complex and characterized by a number of superimposed, relatively weak rotational lines which normally appear as a single broad unresolved feature in the spectrometer pass band due to pressure broadening (Fig. 1, top panel). The strongest emission lines among those observed here are enclosed in the frequency range 269.172–269.452 GHz, and are all within 30 to 100 MHz from one another. In the spectral window sampled by the GBMS for measuring HNO₃, the wing of a strong ozone line is also observed. This O₃ line is centered at 267.266 GHz, outside the GBMS pass band, and contributes background curvature to the HNO₃ spectra that has to be taken into account in the retrieval process. Long integration time (3–5 h, depending on weather conditions) is typically needed to get a satisfactory signal-to-noise ratio for the weak HNO₃ emission spectra.

The two HNO₃ spectra (with the O₃ background superimposed) shown in Fig. 1 are representative of the GBMS measurements at the South Pole. In the top panel a typical spectrum observed during fall is shown, when the largest concentrations of nitric acid are recorded, whereas the spectrum depicted in the bottom panel is measured during polar winter, when HNO₃ has been significantly depleted from the lower stratosphere by incorporation into polar stratospheric clouds and, at the same time, the amount at higher altitudes is increased through formation in, and descent from, the upper stratosphere (de Zafra et al., 1997). As a result the broadening of each emission line is strongly reduced and individually resolved emission lines become visible.
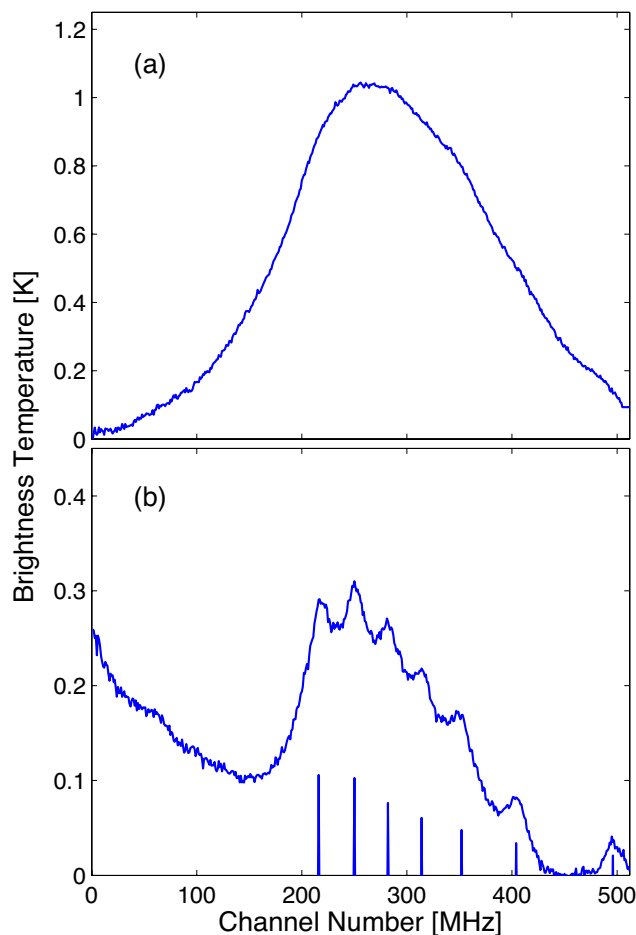

Fig. 1. Representative HNO₃ spectra recorded by the GBMS at South Pole in 1993 during polar fall (15 April) **(a)** and winter (3 August) **(b)**. See text for explanation of the different appearance of these examples. Individual HNO₃ line positions and relative intensities are indicated along the bottom.

3 Forward model

For millimeter wavelengths and temperatures typical of the stratosphere the Rayleigh-Jeans approximation ($h\nu \ll kT$) to the Plank radiation law is valid and the intensity of the observed spectra can be expressed in units of brightness temperature as (e.g., Janssen, 1993):

$$T^*(\nu, z_0) = \int_{z_0}^{\infty} K(\nu, z)\rho(z)dz \tag{1}$$

where

$$K(\nu, z) = T(z)\alpha(\nu, z)e^{-\tau(\nu, z_0)} \tag{2}$$

are weighting functions relating the number density of the emitting species $\rho(z)$ to the emission spectra $T^*(\nu, z_0)$.

The term

$$\tau(\nu, z_0) = \int_z^{z_0} \alpha(\nu, z') \rho(z') dz' \tag{3}$$

represents the self-absorption of the downward propagating emission signal by the species being observed and $\alpha(\nu, z)$ is the absorption coefficient for a single molecule of the species in question. The absorption coefficient is a function of the line shape $\varphi(\nu)$ and of the line intensity $I(T)$, which depends on the population of the lower energy state and thus on the temperature profile:

$$\alpha(\nu, z) = I(T(z))\varphi(\nu, z) \tag{4}$$

The line shape function accounts for the total broadening of the line and has two primary components, due to collisions of the emitting molecule with air molecules and to the Doppler effect. In the altitude range of our observations the only significant effect is pressure broadening. The pressure-broadened line's half-width $\Delta\nu$ is given by:

$$\Delta\nu = \gamma(T_0) \left[\frac{P(z)}{P_0}\right] \left[\frac{T(z)}{T_0}\right]^\chi \tag{5}$$

where T_0 and P_0 are, respectively, a standard reference temperature and pressure, $\gamma(T_0)$ is a collisional broadening coefficient at T_0, and χ is the power law coefficient (typically $\chi < 1$) for the temperature dependence of pressure broadening for a given species. The line shape is well-described by a Lorentzian profile (which accounts only for pressure broadening).

Equations (1) to (5) constitute the forward model that describes the physics of the measurement, and provides the relation between the atmospheric state and the measured spectrum. Atmospheric pressure and temperature profiles, needed in the forward model implementation used for GBMS retrievals, were obtained from the National Center for Environmental Prediction (NCEP) reanalysis for the specific dates and locations. For calculation of absorption coefficients we used lines intensities from the Jet Propulsion Laboratory (JPL) spectral catalog (available at http://spec.jpl.nasa. gov) (Petkie et al., 2003), the pressure broadening coefficients $\gamma(T_0)$ from HITRAN2008 database (http://www.cfa. harvard.edu/hitran) (Rothman et al., 2009) and the temperature dependence exponents χ from Goyette et al. (1991) (see also de Zafra et al., 1997, and references therein).

4 OE retrievals

The retrieval of trace gases vertical profiles from spectral line shapes is an under-constrained problem, meaning that there is an (altitude dependent) envelope within whose boundaries lie many possible profiles which form mathematically acceptable solutions for a given measured line shape, even in the absence of uniform ("white") noise or spectral baseline artifacts. The total integrated intensity under an observed (noise free) spectral line does however put an absolute constraint on the total number of molecules of the observed species along the line of sight through the atmosphere, therefore solutions placing more molecules at one altitude must compensate with fewer at adjacent altitudes, creating the above-mentioned envelope of acceptable concentration vertical profiles. Thermal background, or more precisely the signal-to-noise ratio in the spectrum, reduces the amount of information that can be retrieved from the spectra however, broadening the envelope of possible solutions. In the OE approach, an a priori mixing ratio profile, representing the available information on the species in question at the time of the measurement, provides additional independent information used to select the best retrieval solution from all the possible ones. We discuss this problem of a priori selection in more detail in Sects. 4.1 and 4.2 below.

The OE method is a generic algorithm for solving inverse problems (Rodgers, 1976, 2000), widely employed in atmospheric remote sensing (e.g., Nedoluha et al., 1995; Haefele et al., 2009). This technique has been found to be useful for the analysis of spectra in which signatures of different atmospheric constituents overlap significantly (e.g., Kuntz et al., 1999, and references therein). In our case, the OE is therefore able to simultaneously retrieve both the HNO₃ and the O₃ profiles.

Assuming an atmospheric profile $\boldsymbol{x}$, a synthesized spectrum $\boldsymbol{y}$ can be generated using the forward model $\boldsymbol{F}$:

$$\boldsymbol{y} = \boldsymbol{F}(\boldsymbol{x}, \boldsymbol{b}) + \boldsymbol{\varepsilon} \tag{6}$$

where the vector $\boldsymbol{b}$ contains a set of additional parameters (such as temperature and pressure profiles, spectroscopic parameters etc.) and $\boldsymbol{\varepsilon}$ represents the measurement noise. In our implementation $\boldsymbol{x}$ is an unknown state vector consisting of profiles for two atmospheric constituents (HNO₃ and O₃) that are assumed to be uncorrelated.

Equation (6) can be re-formulated into a simplified form by linearising the forward model about some assumed reference state $\boldsymbol{x}_a$:

$$\boldsymbol{y} - \boldsymbol{F}(\boldsymbol{x}_a) = \frac{\partial \boldsymbol{F}(\boldsymbol{x}, \boldsymbol{b})}{\partial \boldsymbol{x}}(\boldsymbol{x} - \boldsymbol{x}_a) + \boldsymbol{\varepsilon} = \mathbf{K}(\boldsymbol{x} - \boldsymbol{x}_a) + \boldsymbol{\varepsilon} \tag{7}$$

where $\mathbf{K}$ is the weighting function matrix, describing the spectral line shape sensitivity to changes in the different profile elements.

The approach used in the OE is one of combining the measurements ($\boldsymbol{y}$) and the a priori profile ($\boldsymbol{x}_a$) information together, with assigned weights derived from the respective inverse covariances $\mathbf{S}_\varepsilon$ and $\mathbf{S}_a$. The retrieval solution is given by:

$$\hat{\boldsymbol{x}} = \boldsymbol{x}_a + \left(\mathbf{K}^T \mathbf{S}_\varepsilon^{-1} \mathbf{K} + \mathbf{S}_a^{-1}\right)^{-1} \mathbf{K}^T \mathbf{S}_\varepsilon^{-1} (\boldsymbol{y} - \mathbf{K}\boldsymbol{x}_a) \tag{8}$$

where

$$\hat{\boldsymbol{x}} = \begin{pmatrix} \hat{\boldsymbol{x}}_{HNO_3} \\ \hat{\boldsymbol{x}}_{O_3} \end{pmatrix}; \quad \boldsymbol{x}_a = \begin{pmatrix} \boldsymbol{x}_{a_{HNO_3}} \\ \boldsymbol{x}_{a_{O_3}} \end{pmatrix}; \quad \mathbf{S}_a = \begin{pmatrix} \mathbf{S}_{a_{HNO3}} & 0 \\ 0 & \mathbf{S}_{a_{O3}} \end{pmatrix}$$

$\hat{x}_{\text{HNO}_3}$, $x_{\text{a}_{\text{HNO}_3}}$, $\mathbf{S}_{\text{a}_{\text{HNO}_3}}$ and $\hat{x}_{\text{O}_3}$, $x_{\text{a}_{\text{O}_3}}$, $\mathbf{S}_{\text{a}_{\text{O}_3}}$ represent the retrieved profile, the a priori profile and the a priori covariance matrix for nitric acid and ozone, respectively.

Due to self-absorption, the brightness temperature of the downward propagating stratospheric signal is a non-linear function of the vertical distributions of the emitting species. In practice, however, due to the low concentration of HNO₃ in the stratosphere, we can consider it to be a linear problem with the weighting functions evaluated at $\rho(z) = \rho_{\text{a}}(z)$. To check whether this approximation is adequate, we determined the degree of nonlinearity of the problem. According to Rodgers (2000) the error introduced on the retrieval solution using a linear approximation can be estimated by:

$$\partial \hat{x} = \mathbf{G}\big[\mathbf{F}(\hat{x}) - \mathbf{F}(x_{\text{a}}) - \mathbf{K}(\hat{x} - x_{\text{a}})\big] \qquad (9)$$

where

$$\mathbf{G} = \left(\mathbf{K}^T \mathbf{S}_\varepsilon^{-1} \mathbf{K} + \mathbf{S}_{\text{a}}^{-1}\right)^{-1} \mathbf{K}^T \mathbf{S}_\varepsilon^{-1} \qquad (10)$$

In our implementation this error is at most $\sim$0.5 % of the mixing ratio retrieved profile. Additionally, a sample of HNO₃ spectra were deconvolved using both the linear and the non-linear (iterative) approaches and a negligible difference of at most 0.05 % of the mixing ratio retrieved profiles was observed, reinforcing the validity of the linear approximation.

4.1 A priori information

As outlined previously, in our implementation of the OE both the HNO₃ and the O₃ vertical profiles are quantities to be retrieved and a priori profiles for both species have hence to be provided. In fact, the ozone line is no more than a background to the HNO₃ spectrum, containing poor information about O₃ vertical distribution. Ozone profiles are retrieved only in order to allow the measured spectra to be inverted as a whole, avoiding a preliminary subtraction process, and are not used for ozone retrieval. For this reason, the retrieval of ozone relies almost completely on the a priori information that therefore needs to be as accurate as possible. We obtain this information from ozonesonde data which are generally available for the locations where the GBMS has been operated. Although balloon profiles usually extend only up to $\sim$30 km, they are well suited for our purpose since the emission of the observed O₃ line wing arises entirely from O₃ molecules located at altitudes below 30 km.

A priori information for the retrieval of HNO₃ profiles were obtained from the NASA/JPL Microwave Limb Sounder (MLS) experiment aboard of the EOS Aura satellite from 2004 to date (Waters et al., 2006; Santee et al., 2007). Given the latitudinal dependence of the HNO₃ vertical distribution, a different a priori profile was considered for each observation site where the GBMS has been deployed. For Testa Grigia, where the GBMS was operated for 4 winter periods, from 2004 to 2007, and Thule, where observations were carried out during polar winters 2008/2009, 2009/2010, and 2010/2011 concurrent MLS data are available. We averaged together all the MLS HNO₃ vertical profiles obtained during the GBMS observation periods within 2.5° latitude and 10° longitude from each observing site. A smoothing was then applied in order to remove fine vertical structures in the MLS mean profiles. For GBMS measurements obtained at the South Pole in 1993 and 1995, the first generation of MLS was operating, aboard the Upper Atmosphere Research Satellite (UARS). However, the use of UARS/MLS measurements as a priori for GBMS South Pole retrievals would have two major drawbacks: (1) UARS/MLS has a limited coverage of the extreme polar regions, reaching a southernmost latitude of only about 80° and switching monthly between viewing northern and southern high latitudes; (2) UARS/MLS HNO₃ measurements are less reliable than Aura MLS data, especially in polar winters, with potential biases as large as 4–5 ppbv inside the vortex (Livesey et al., 2003). In light of the above points and considering that we are interested in an a priori profile containing information on the mean HNO₃ distribution in a certain region rather than on the HNO₃ profile for a specific date or year, the a priori profile for the South Pole GBMS measurements was built using Aura MLS measurements south of 80° S during the first two years of MLS operations (2005 and 2006). The same smoothing procedure described for Testa Grigia and Thule was followed in this case. Since the HNO₃ distribution shows a strong seasonal variation at polar latitudes, a full year cycle of GBMS measurements was divided in 6 2-month periods and a different a priori profile was used for each period. Mean MLS profiles obtained with this procedure provide adequate information on the typical behavior of the HNO₃ throughout the year at the South Pole.

4.2 Covariance matrices

$\mathbf{S}_{\text{a}}$ and $\mathbf{S}_\varepsilon$ are the covariance matrices of the a priori mixing ratio profile and of the measured spectrum whose diagonal elements, designated with σ_{a}^2 and σ_ε^2, are the variances of the single elements of the corresponding vectors. The off diagonal elements indicate a cross-correlation between the corresponding elements of each vector. If they are nonzero then a correlation exists and we have more information about the vector than we have for the case of negligible off-diagonal elements. The selection of these variances is one of the most critical points in tuning the retrieval method in order to obtain reliable retrievals, determining the amount of information the measurement actually adds to that provided by the a priori profile. In fact, very small errors in the a priori profile strongly constrain the retrieved profile to the a priori information, while large σ_{a} values lead to solutions relying mostly on the spectral measurement and with a tendency to oscillate.

Following the classical formulation of the Optimal Estimation method, the diagonal elements of $\mathbf{S}_{\text{a}}$ should be derived from an accurate estimate of the true variability of HNO₃
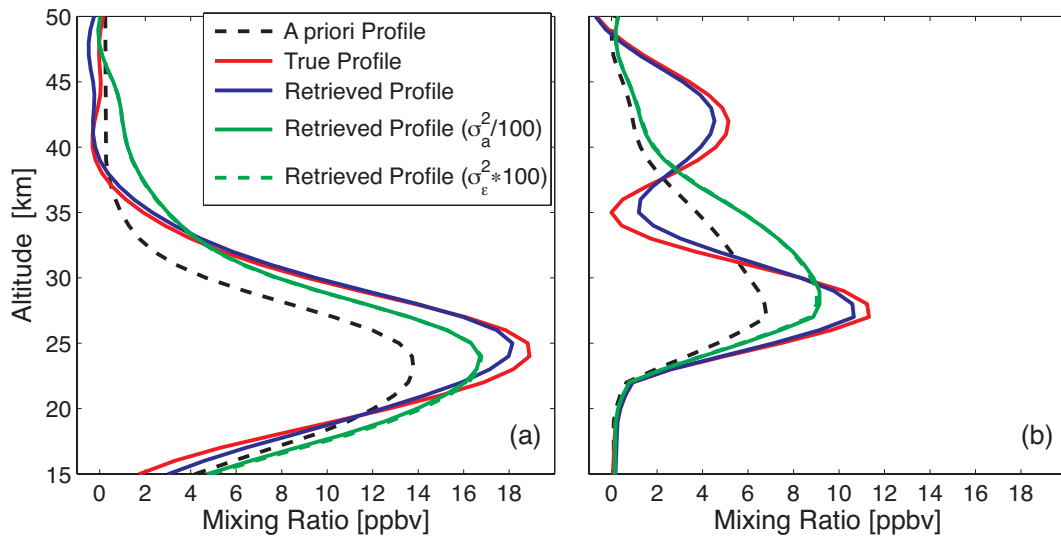
Fig. 2. Profile retrievals of HNO₃ synthetic spectra forward-simulated starting from two typical HNO₃ distributions that could be observed at polar regions during late fall **(a)** and winter **(b)**. Retrieved results obtained using selected σ_ε^2 and σ_a^2 values are shown (blue line) together with a priori profiles (dashed black line) and "true" synthetic vertical profiles (red line). Retrieval results obtained increasing σ_ε^2 by a factor 100 (dashed green line) and decreasing σ_a^2 of the same factor (solid green line) are also shown.

mixing ratio at different altitudes. As for the diagonal elements of $\mathbf{S}_\varepsilon$, a theoretical estimate of the thermal noise in the calibrated spectra can be computed according to the radiometer sensitivity equation (Kraus, 1966):

$$\sigma_\varepsilon = \frac{2T_{\text{sys}}}{\sqrt{\delta\nu\delta t}} \qquad (11)$$

where T_{sys} is the system temperature (including the receiver noise temperature and the brightness temperature due to the tropospheric continuum), $\delta\nu$ is the bandwidth of a given channel and δt is the integration time (see also Parrish et al., 1988; de Zafra, 1995). However, this value often underestimates the actual spectral noise and a more realistic value is provided by the square of the rms of the spectral residuals (i.e., the differences between the measured spectra and those generated from the retrieved profiles using the forward model) (Parrish et al., 1992).

In practice, in many semi-empirical versions of the method (Parrish et al., 1992; Nagahama et al., 1999), both these matrices are treated as adjustable parameters whose values are set empirically by optimizing the performance of the retrieval process in order to have the best possible resolution without introducing ambiguous oscillations in the solutions. Since the retrieval performance is determined by the relative weight of the information coming from the a priori profile and from the measurements (namely by the $\mathbf{S}_a$ to $\mathbf{S}_\varepsilon$ ratio rather than by their absolute values, see later discussion on Fig. 2), for GBMS HNO₃ retrievals we decided to fix the uncertainty on the a priori profile (using, in fact, its most realistic estimate) and to use $\mathbf{S}_\varepsilon$ as adjustable parameter for optimizing the retrieval sensitivity. The $\mathbf{S}_a$ to $\mathbf{S}_\varepsilon$ ratio can vary from site to site,

just like the a priori profile, due to different characteristics of the data set (e.g., signal to noise ratio, intensity of the background ozone line, etc.). Additionally, a correlation between gas concentrations at different altitudes is enforced, with the off-diagonal elements expressing this correlation given by:

$$S_{a_{i,j}} = \sigma_{a_i}\sigma_{a_j}\exp\left\{-|z_i - z_j|\frac{1}{h}\right\} \qquad (12)$$

where z_i is the i-th altitude level, $\sigma_{a_i}^2$ is the corresponding variance, and h is the correlation length, which is assumed to be 5 km over the whole atmosphere for both O₃ and HNO₃ (Hoogen et al., 1999).

Since there is no significant channel to channel correlation in the spectrum and the thermal noise at each channel is approximately the same, $\mathbf{S}_\varepsilon$ is assumed to be a diagonal matrix with all the diagonal elements, σ_ε^2, equal. The value of the diagonal elements was determined empirically by performing a set of inversions on observed and simulated spectra. First of all, we forward-generated several synthetic spectra starting from arbitrary, reasonable (hereafter referred to as true) O₃ and HNO₃ profiles and we inverted these simulated spectra using different σ_ε values. Afterwards, the variance values which provided solutions matching well the true profiles were used to invert measured spectra. Some of these σ_ε produced retrieved profiles displaying unrealistic oscillations. As GBMS HNO₃ spectra may change significantly in shape (e.g., Antarctic fall versus winter) or S/N ratio (e.g., polar versus middle latitudes) depending on observing site and season, we divided the whole data set in different subsets and for each subset adopted the smallest σ_ε value (corresponding to the highest resolution) which did not lead to

unphysical solutions. The σ_ε^2 eventually adopted in the various cases studied are of the same order of magnitude of the spectral residuals that characterize the HNO$_3$ spectra from the different observing sites.

Two examples from these retrieval tests are presented in Fig. 2. True synthetic vertical profiles and retrieval results obtained using selected σ_ε and σ_a values are shown, together with a priori profiles. The first true profile (Fig. 2a) represents a typical HNO$_3$ distribution that could be observed in polar regions during late fall. In the figure, retrieved profiles that were obtained by increasing σ_ε^2 by a factor 100 and decreasing σ_a^2 by the same amount are also shown. These tests confirm that increasing measurement errors or decreasing a priori uncertainties by the same factor leads to analogous solution profiles, closer to the a priori and with their corresponding spectra (not shown) displaying a poorer agreement with the observed spectrum. Figure 2b shows analogous tests run using an HNO$_3$ synthetic true profile typical of the denitrification process, which takes place in the Antarctic vortex during winter.

4.3 Characterization of the retrieval

A useful quantity to characterize the retrieval sensitivity to changes in the true atmospheric state is represented by the AK matrix $\mathbf{A}$:

$$\mathbf{A} = \frac{\partial \hat{\boldsymbol{x}}}{\partial \boldsymbol{x}} = \left(\mathbf{K}^T \mathbf{S}_\varepsilon^{-1} \mathbf{K} + \mathbf{S}_a^{-1}\right)^{-1} \mathbf{K}^T \mathbf{S}_\varepsilon^{-1} \mathbf{K} \qquad (13)$$

The rows of $\mathbf{A}$ represent the AKs, whereas the columns are known as the delta-function responses (DRs).

The AK $\left(\frac{\partial \hat{x}_i}{\partial \boldsymbol{x}}\right)$ represents the response of the retrieval at the i-th altitude to a unit perturbation in all elements of the true atmospheric state, while the DR $\left(\frac{\partial \hat{\boldsymbol{x}}}{\partial x_j}\right)$ shows how the whole retrieved profile responds to a delta-perturbation of the true profile at level j. In the ideal case, $\mathbf{A}$ is the unit matrix. In fact, rows of $\mathbf{A}$ are peaked functions, with the full width at half maximum (FWHM) of each providing an estimate of the local vertical resolution of the retrieved profile.

Using the matrix $\mathbf{A}$, the solution can be rewritten in the following form:

$$\hat{\boldsymbol{x}} = \boldsymbol{x}_a + \mathbf{A}(\boldsymbol{x} - \boldsymbol{x}_a) \qquad (14)$$

showing that the retrieved profile at each altitude consists of an a priori value at the corresponding altitude plus the deviation of the true profile from the a priori, smoothed with the associated AK.

One further useful quantity in the retrieval characterization is the contribution of the a priori to the retrieved profile, defined by Connor et al. (1995) as

$$\sum_j (\mathbf{I} - \mathbf{A})_{i,j} x_{a_j} / \hat{x}_i \quad . \qquad (15)$$

This quantity provides an important, albeit rough, estimate of the degree of dependence of the retrieved mixing ratio values

from the a priori profile. From Eq. (15), it appears that this parameter can have positive or negative values since most off-diagonal elements of $(\mathbf{I}-\mathbf{A})_{i,j}$ are negative and work to "balance" the contribution of the positive diagonal elements (see also, e.g., Fig. 7 in Connor et al., 1995). Furthermore, when the retrieved profile $\hat{x}_i$ (at the denominator of Eq. 15) has nearly zero values (top and bottom altitudes of the GBMS HNO$_3$ retrievals), the a priori contribution can run off to large positive or negative values. For the purpose of evaluating the altitude range where the retrieved HNO$_3$ profile can be considered reliable, only the absolute value (not its sign) of the a priori contribution is a useful information.

Figure 3a, b and c shows, respectively, typical GBMS AKs, vertical resolution values (the FWHM of the AKs), and contributions of the a priori profile for winter mid-latitude observations carried out at Testa Grigia. It is perhaps useful to point out that numerous tests have shown that the inversion technique locates the maximum of the HNO$_3$ mixing ratio vertical profile (as well as that of other species) with a much better accuracy (i.e., $\sim \pm 1$ km) than might casually be supposed by inspection of the FWHM of the AKs appropriate to the altitude of maximum mixing ratio (see Fig. 2a and b). The integrated area under each delta-function response, representing the total sensitivity of the retrieval to delta perturbations in the true atmosphere at the respective altitude, is also shown (reduced by a factor 10) in Fig. 3a (dashed black line). Figure 3d–f and 3g–i shows the same parameters for measurements obtained at the South Pole during fall and winter seasons (note that in Fig. 3g the horizontal scale is different). The three sets of AKs are obtained with similar σ_a (~ 1.5 ppbv) and values of σ_ε of 2.5×10^{-3}, 2.5×10^{-4}, and 1.25×10^{-5} for the AKs in Fig. 3a, d, and g, respectively. These different settings were chosen in order to extract the maximum amount of information from the measured spectra of each data set, without however producing oscillatory results. The AKs are quite similar in the case of mid-latitudes winter and Antarctic fall observations (Fig. 3a and d, respectively). Both sets are well peaked and centered close to their correct altitude level (i.e., the j-th column of the averaging kernel matrix has its maximum value at the i-th row, with $i = j$) in the middle stratosphere, with their sensitivity close to 1. However, due to a better S/N ratio of the Antarctic fall spectra, which allows us to use lower σ_ε values in the retrieval, a higher vertical resolution (between 9 and 12 km below 43 km altitude) and an overall better performance in the upper stratosphere is obtained for Antarctic fall with respect to mid-latitudes profiles. Due to the peculiar features of the emission spectra observed during the Antarctic winter (Fig. 1b), the associated AKs are rather different with respect to the other two sets. In winter, each HNO$_3$ emission line in the GBMS spectral window can be clearly observed and this allowed us to further reduce σ_ε, producing sharper AKs (Fig. 3g) and improved vertical resolutions (Fig. 3h). On the other hand, the extremely low HNO$_3$ concentrations at altitudes affected by the denitrification process strongly reduce
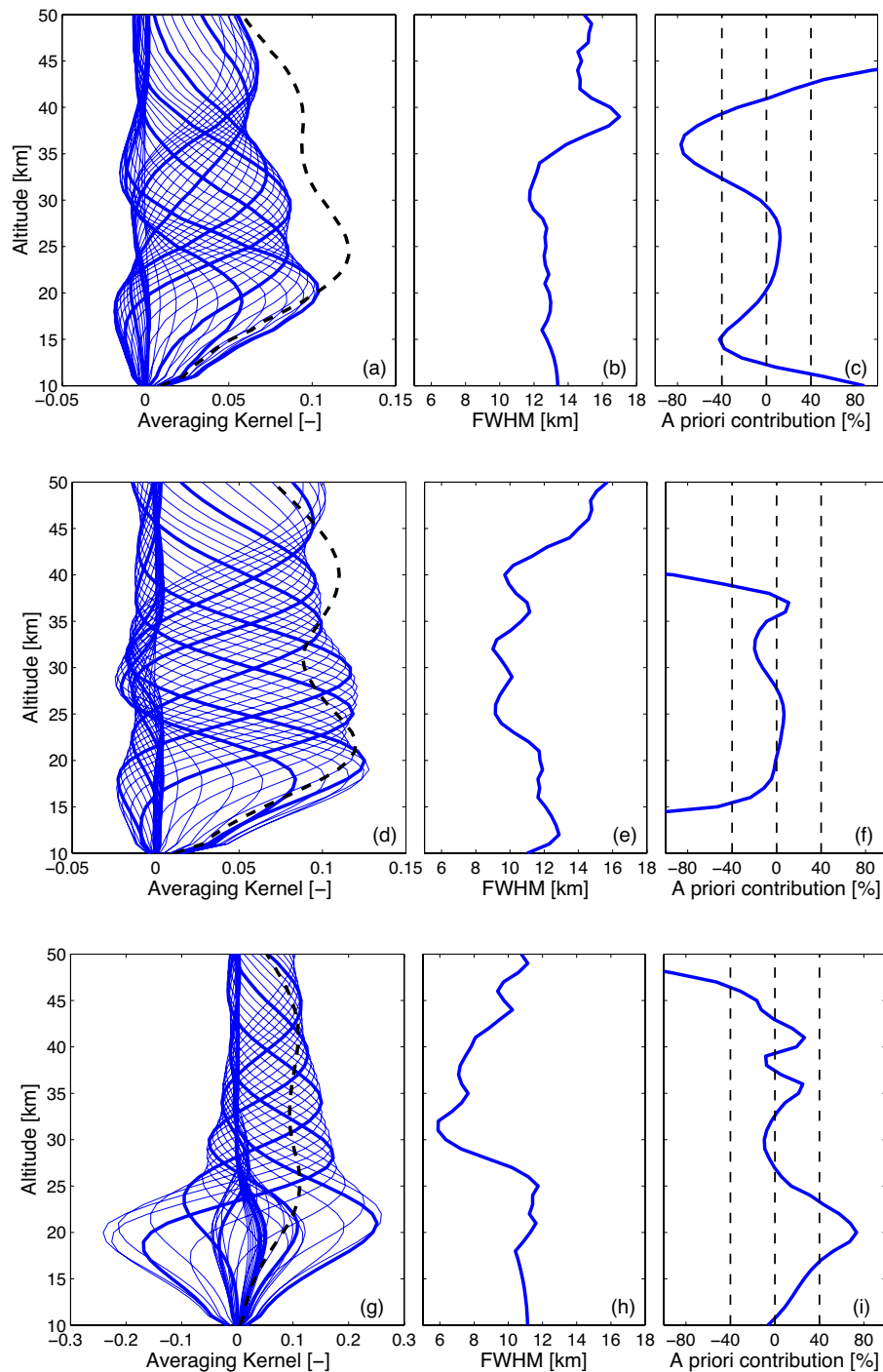
Fig. 3. GBMS averaging kernels (**a**, **d**, and **g**), retrievals vertical resolution (**b**, **e**, and **h**), and a priori contribution (**c**, **f**, and **i**) for three different cases: winter mid-latitudes observations at Testa Grigia (panels **a**–**c**), high-latitude observations at South Pole during fall (panels **d**–**f**) and winter (panels **g**–**i**). The three sets of AKs are obtained with $\sigma_a \sim 1.5$ ppbv and values of σ_ε of 2.5×10^{-3} (panel **a**), 2.5×10^{-4} (panel **d**), and 1.25×10^{-5} (panel **g**). In panels (**a**), (**d**), and (**g**), thicker blue lines are averaging kernels calculated each 5 km, from 15 to 45 km, whereas dashed black lines represent the total sensitivity, as defined in the text, divided by 10.

emissions at the individual HNO₃ spectral line wings (containing the information on lower altitudes) which tend to become difficult to separate from baseline distortion due to the

ozone background line. This produces the large oscillations in AKs at lower altitudes, where the AKs correspondent to the 30–35 km range display secondary negative peaks located

at ~20–25 km, implying that positive variations of HNO$_3$ concentrations at 20–25 km altitude will affect negatively the retrieval values at 30–35 km. It is worth stressing, however, that this reduced sensitivity in the winter lower stratosphere is due to nearly zero HNO$_3$ values. Several tests, simulating layers of HNO$_3$ brought by the evaporation at these altitudes of PSC particles (renitrification), showed that the overall uncertainty in retrieved mixing ratio values in the lower stratosphere is the larger of ~50 % or 0.1 ppbv. Furthermore, as soon as HNO$_3$ mixing ratios return to non negligible values in spring, the sensitivity returns to satisfactory levels.

Figure 3c, f and i shows that the contribution of the a priori profile to the derived mixing ratio profile is generally lower than 40 % at altitudes where the sensitivity parameter is near 100 %. Although the a priori contribution is a parameter widely used in the literature, its drawback is that depends significantly on the choice of the a priori and on the retrieved vertical profile (see Eq. 15). As discussed earlier, this can cause the a priori contribution to have discontinuities or large oscillations even at altitudes where the inversion algorithm proves to have a good sensitivity to the spectral measurements. For this reason we use the sensitivity parameter as an additional tool for characterizing capabilities and limits of the retrieval technique.

4.4 Error estimate

Uncertainties in the retrieved nitric acid profiles are due to different sources: instrument calibration, forward parameters, measurements noise and smoothing errors. Those related to calibration procedure (e.g., errors in receiver temperature and atmospheric opacity estimate) and to parameters used in the forward model calculation (e.g., spectroscopic parameters, pressure and temperature vertical profiles) have been estimated to add up to 15 % (de Zafra et al., 1997; Muscari et al., 2002), with a contribution of 8 % from systematic errors. In changing the inversion technique from MI to OE, measurements noise has been assessed according to Connor et al. (1995), which expresses the profile error covariance due to the error in spectral measurements as:

$$\mathbf{S}_n = \mathbf{G}\mathbf{S}_{\varepsilon'}^{-1}\mathbf{G}^T \qquad (16)$$

Here $\mathbf{S}_{\varepsilon'}$ is a diagonal matrix with the diagonal elements given by the squares of the spectral residuals. Equation (16) allows mapping of the spectral noise from the measurements space to the profile space, using the contribution functions $\mathbf{G}$ defined in Eq. (10). The smoothing error accounts for the fact that fine vertical structure of the atmospheric state cannot be resolved in the retrieved profile, due to the limited vertical resolution of the observing technique. The associated covariance matrix is:

$$\mathbf{S}_s = (\mathbf{A} - \mathbf{I})\mathbf{S}_a(\mathbf{A} - \mathbf{I})^T \qquad (17)$$

When comparing GBMS profiles to other data sets, the higher-resolution measurement profile $\boldsymbol{x}_{\text{hr}}$ is convolved with
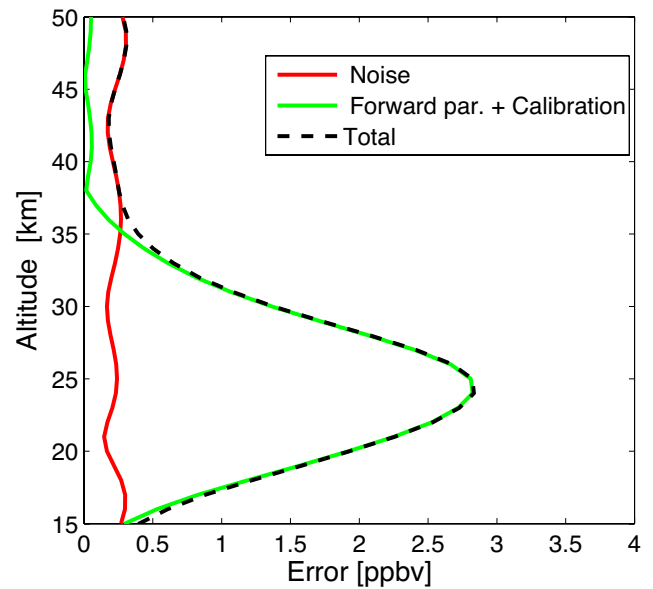

Fig. 4. Estimated errors on the retrieved Antarctic fall profile presented in Fig. 5. The various sources of error are: calibration and forward parameters (green line) and measurement noise (red line). The total uncertainty is also shown (dashed black line).

the lower-resolution measurement AKs matrix, $\mathbf{A}_{\text{lr}}$ and the smoothing error should not be considered. According to Eq. (14) the smoothed (or convolved) profile is given by:

$$\hat{\boldsymbol{x}}_{\text{smo}} = \boldsymbol{x}_{\text{a}} + \mathbf{A}_{\text{lr}}(\boldsymbol{x}_{\text{hr}} - \boldsymbol{x}_{\text{a}}) \qquad (18)$$

A correct evaluation of the smoothing error requires, however, an accurate knowledge of the variability of the fine structure of the true atmosphere (Rodgers, 2000; Connor et al., 1995). Due to this strict requirement, the smoothing error is rarely considered in the literature on the OE method and we do not include it in our error estimate. Figure 4 shows the contributions of the different uncertainties described above to the total 1σ error on the Antarctic fall profile presented in Fig. 5 (for Antarctic winter profiles, not shown, relative contributions and total uncertainty are slightly different). The measurement error covariance matrix, $\mathbf{S}_n$, has nonzero off-diagonal elements, suggesting that the errors at different levels are correlated. Since visualizing correlated errors can be quite difficult, the uncertainties presented in Fig. 4 have been calculated as the square root of the diagonal elements of the covariance matrix, neglecting the correlations between adjacent layers. This approach means that we are, at worst, overestimating the uncertainties. The total uncertainty on the retrieved profiles, determined by adding in quadrature the errors due to the different sources, is generally given by the larger of 15 % or 0.3 ppbv (dashed black line in Fig. 4), with small differences depending on observing sites and conditions.
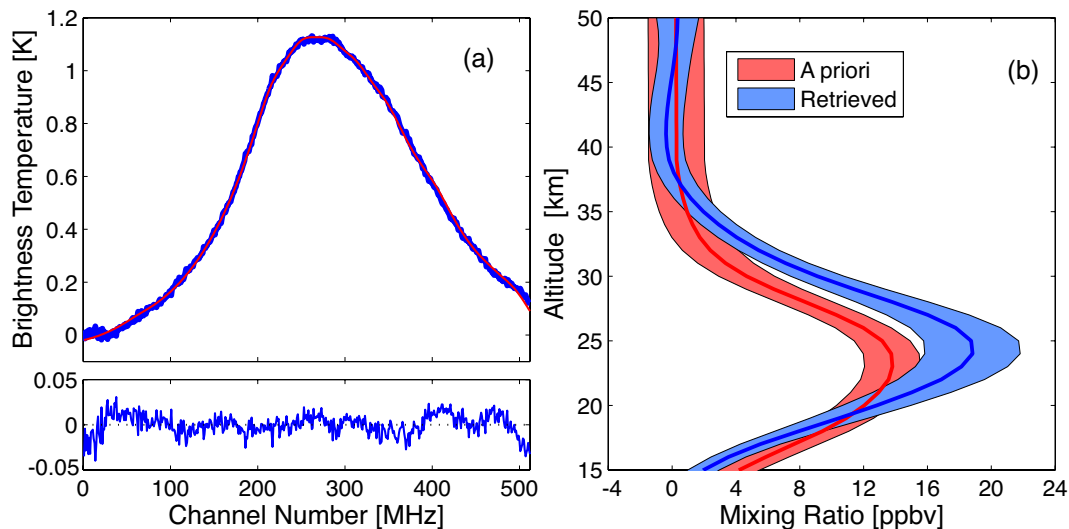
Fig. 5. (a) HNO$_3$ spectrum observed by the GBMS on 28 April from the Amundsen Scott Base at South Pole. The superimposed red line is the spectrum forward-generated from the retrieved profile. In the bottom panel the spectral residuals (measured spectrum minus calculated spectrum) are shown. **(b)** HNO$_3$ profile retrieved from the GBMS spectrum shown in panel **(a)**. The a priori profile used in the retrieval is also shown (red line). Red and blue shaded areas are, respectively, uncertainties on the a priori profile considered in the retrieval and estimated total error on the retrieved profile.

5   Comparison between OE and MI HNO$_3$ retrievals

Until recently the GBMS HNO$_3$ spectra were processed using the MI technique (de Zafra et al., 1997). The MI is an iterative method, essentially immune to the choice of the a priori profile used to start the iteration, employing a vertical smoothing algorithm to constrain the solution (Twomey, 1977). However, the lack of straightforward AKs in the MI method made it difficult to consistently compare GBMS observations to data sets with a higher vertical resolution, such as in situ measurements or measurements carried out by instruments aboard recent satellite missions.

We have therefore compared HNO$_3$ profiles retrieved with the OE (v2) and the MI (v1) methods to evaluate how the change in retrieval algorithm might affect previous comparison works using the GBMS MI-based HNO$_3$ retrievals (Muscari et al., 2002; Santee et al., 2007; Fiorucci et al., 2009), and at the same time to provide a preliminary evaluation of the HNO$_3$ v2 dataset. This comparison is presented in Fig. 6 for three cases illustrative of the most diverse conditions encountered, concerning both the S/N ratio of spectra (closely related to a site typical atmospheric opacity) and the HNO$_3$ stratospheric concentrations (varying dramatically especially from Antarctic fall to winter). These cases are: winter mid-latitude observations carried out at Testa Grigia in 2005 (Fig. 6a–b), high-latitude measurements carried out at South Pole in 1993–1995 during the fall (Fig. 6c–d) and winter seasons (Fig. 6e–f). Each case is illustrated by means of averaged profiles obtained by using all the available GBMS HNO$_3$ profiles for the specific time period and location (13 profiles for Testa Grigia 2005, 5 profiles for 1993 and 1995

South Pole fall, and 16 profiles for 1993 and 1995 South Pole winter). Data from the 2006 and 2007 observing campaigns at Testa Grigia were not used in this study for consistency with the MLS validation paper of Santee et al. (2007) based on 2005 GBMS HNO$_3$ profiles. Furthermore, their addition would not add any information to or display any difference with the results shown in Fig. 6a–b. In Fig. 6, left panels show mean profiles retrieved by means of the OE and the MI techniques while their absolute differences are shown in right panels. At Testa Grigia, HNO$_3$ profiles retrieved with the MI are systematically larger near the peak than those obtained with the OE, with differences up to ∼1.5–2 ppbv. A similar behavior is observed for the South Pole fall data set, with a high bias of the MI retrieved profiles in the mixing ratio peak region of about 1.5 ppbv. Conversely, the only significant (i.e., non-overlapping error estimates) difference between v1 and v2 retrievals of the winter South Pole data set are observed in the upper stratosphere, near 40 km. These results suggest that changing the retrieval method might affect the retrieved profiles differently depending on the shape of the observed spectra, i.e., depending on the vertical distribution of the trace gas observed.

As mentioned above, GBMS HNO$_3$ measurements discussed here had been previously compared to satellite observations obtained from the NASA/JPL MLS experiments onboard of UARS and EOS Aura satellites. According to this comparison, GBMS HNO$_3$ measurements carried out at Testa Grigia in 2005 were biased toward higher mixing ratios with respect to Aura MLS v2.2 HNO$_3$ profiles by as much as 3 ppbv (20–30 %) near the peak (Santee et al., 2007). Santee
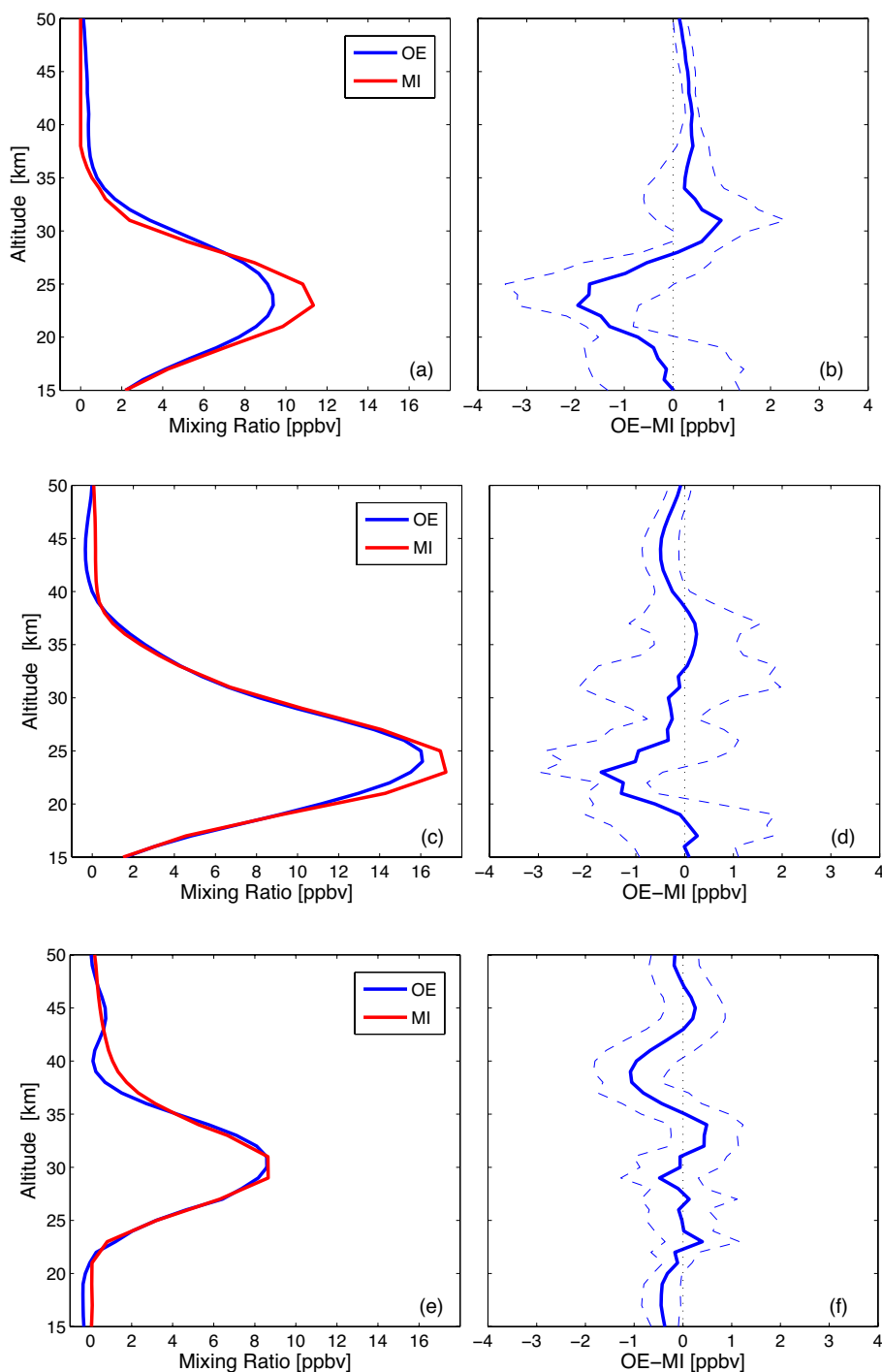
Fig. 6. Left panels: comparison between HNO$_3$ profiles retrieved with the constrained Matrix Inversion (red line) and the Optimal Estimation (blue line) techniques. Right panels: absolute differences between the profiles retrieved using the two different techniques. Dashes lines are standard deviations of these differences. The comparison is presented for three illustrative cases: 2005 winter at Testa Grigia (13 days) (panels **a** and **b**), 1993–1995 fall at South pole (5 days) (panels **c** and **d**), 1993–1995 winter at South Pole (16 days) (panels **e** and **f**).

et al. (2007), however, also reported a low bias of MLS v2.2 HNO$_3$ profiles of ∼1 ppbv at the mixing ratio peak with respect to other satellite datasets.

A similar high bias (2–3 ppbv) was observed in the GBMS HNO$_3$ 1993 polar fall measurements with respect to the UARS MLS v5 HNO$_3$ data, in the range 20–27 km (Muscari

et al., 2002). During winter, in the same altitude range, with a denitrified lower stratosphere, the same comparison displayed GBMS values lower than MLS mixing ratios by 1–2 ppbv, and this difference was ascribed in Muscari et al. (2002) to non linearities in the MLS retrieval system temperatures.

According to the differences observed between GBMS HNO₃ v1 and v2 retrievals, it appears that v2 profiles are in better agreement with MLS data sets with respect to that shown by v1 profiles in previous comparisons. Preliminary studies (Fiorucci et al., 2009) comparing GBMS v2 and Aura/MLS v3 HNO₃ vertical profiles at Testa Grigia support this result. Version 2 profiles bring no improvement in the Antarctic winter case, where, however, lower stratospheric differences between GBMS and MLS measurements are likely due to the UARS MLS v5 retrieval system (Muscari et al., 2002). A comprehensive intercomparison between GBMS v2 and Aura/MLS v3 HNO₃ vertical profiles is underway.

6 Summary

The GBMS has acquired a unique long-term ground-based dataset of stratospheric HNO₃ which contributed to our knowledge on Antarctic stratospheric processes (de Zafra et al., 1997; McDonald et al., 2000; Muscari et al., 2003) and to validation of satellite-based data sets (Muscari et al., 2002; Santee et al., 2007). With the aim of a better compliance of GBMS HNO₃ measurements to the NDACC database standards, and in order to establish a long-term stratospheric trace gases observing station in the Arctic, we chose Thule (76.5° N, 68.8° W) as a permanent site for the GBMS, installed it there in January 2009, and developed an Optimal Estimation method for deconvolving GBMS spectra. The OE provides the necessary tools for straightforward and accurate comparisons of GBMS profiles with other data sets, especially if the latter are characterized by a higher vertical resolution with respect to the GBMS. The OE method was applied to all the existing GBMS HNO₃ data (at South Pole in 1993, 1995, and 1999; at Testa Grigia from 2004 to 2007; at Thule from 2009 to date) producing a version 2 set of HNO₃ vertical profiles. Here we described the main characteristics of the OE inversions of GBMS HNO₃ spectra covering locations and temporal windows that offer a wide variety of spectral features, from the very intense emissions during the Antarctic Fall (Fig. 1a) to the emergence of single resolved lines during the lower stratospheric denitrification and the upper stratospheric HNO₃ enhancement processes of Antarctic winter (Fig. 1b) (e.g., de Zafra et al., 1997). Different sites and spectral features cause differences in the averaging kernels of the various sets of GBMS HNO₃ measurements (Fig. 3). In general, v2 profiles show a sensitivity of $100 \pm 20\%$ from ~20 to ~45 km altitude. The total error on HNO₃ v2 mixing ratio vertical profiles is estimated by adding

in quadrature the uncertainties due to forward parameters, instrumental calibration and spectral noise, and their relative contributions (Fig. 4) are also subjected to small changes depending on observing site and season (both affect the S/N ratio and information content of measurements). Generally, the 1σ uncertainty between 15 and 50 km altitude amounts to the larger of 15 % or 0.3 ppbv (Figs. 4 and 5). HNO₃ v2 have been compared to HNO₃ v1 vertical profiles obtained employing the constrained matrix inversion method, during Antarctic fall and winter, and at the mid-latitude site of Testa Grigia (Fig. 6). The two versions agree within their combined uncertainties. During the Antarctic winter their differences are negligible in the 20–35 km altitude range, reaching a maximum difference of less than 1 ppbv at 40 km (Fig. 6e and f). However, at midlatitudes and during the Antarctic fall, v2 profiles are systematically less than v1 at the HNO₃ mixing ratio maximum (20–25 km altitude) by up to 2 ppbv (Fig. 6a–b and 6c–d). Considering the results of Muscari et al. (2002) and Santee et al. (2007), this difference suggests that GBMS HNO₃ v2 profiles have a better agreement with both UARS/ and EOS Aura/MLS HNO₃ data than previous GBMS HNO₃ v1. An intercomparison study between GBMS v2 and Aura/MLS v3 HNO₃ vertical profiles at mid- and high northern latitudes is being undertaken.

References

Brasseur, G. and Solomon, S.: Aeronomy of the middle atmosphere: Chemistry and Physics of the Stratosphere and Mesosphere, D. Reidel Pub. Co., Dordrecht, The Netherlands, 1984.

Connor, B. J., Parrish, A., Tsou, J. J., and McCormick, M. P.: Error analysis for the ground-based microwave ozone measurements during STOIC, J. Geophys. Res., 100(D5), 9283–9291, 1995.

de Zafra, R. L.: The ground-based measurements of stratospheric trace gases using quantitative millimeter wave emission spectroscopy, in Diagnostic tools in atmospheric physics, Proceedings of the international school of physics "Enrico Fermi", 23–54, Società italiana di fisica, Bologna, 1995.

de Zafra, R. L., Chan, V., Crewell, S., Trimble, C., and Reeves, J. M.: Millimeter wave spectroscopic measurements over the South Pole: 3. The behavior of stratospheric nitric acid through polar fall, winter, and spring, J. Geophys. Res., 102(D1), 1399–1410, 1997.

Di Biagio, C., Muscari, G., di Sarra, A., de Zafra, R. L., Eriksen, P., Fiorucci, I., and Fuà, D.: Evolution of temperature, O₃, CO, and N₂O profiles during the exceptional 2009 Arctic major stratospheric warming as observed by lidar and mm-wave spectroscopy at Thule (76.5° N, 68.8° W), Greenland, J. Geophys. Res., 115, D24315, doi:10.1029/2010JD014070, 2010.

Fahey, D., Murphy, D., Kelly, K., Ko, M., Proffitt, M., Eubank, C., Ferry, G., Loewenstein, M., and Chan, K.: Measurements of Nitric Oxide and total reactive nitrogen in the Antarctic stratosphere: observations and chemical implications, J. Geophys. Res., 94(D14), 16665–16681, 1989.

Fiorucci. I., Muscari, G., Bianchi, C., Di Girolamo, P., Esposito, F., Grieco, G., Summa, D., Bianchini, G., Palchetti, L., Cacciani, M., Di Iorio, T., Pavese, G., Cimini, D., and de Zafra, R. L.: Measurements of low amounts of precipitable water vapor by millimeter wave spectroscopy: An intercomparison with radiosonde, Raman lidar, and Fourier transform infrared data, J. Geophys. Res., 113, D14314, doi:10.1029/2008JD009831, 2008.

Fiorucci, I., Muscari, G., Froidevaux, L., Santee, M. L., and De Zafra, R. L.: Establishing a long-term, global stratospheric HNO$_3$ data record combining UARS MLS with Aura MLS data by means of ground-based measurements, AGU Fall Meeting, San Francisco, CA, USA, 14–18 December 2009, A21C-0218, 2009.

Goyette, T. M., Guo, W., and De Lucia, F. C.: Variable temperature pressure broadening of HNO$_3$ in the millimeter wave spectral region, J. Mol. Spectros., 46(4), 293–297, 1991.

Haefele, A., De Wachter, E., Hocke, K., Kämpfer, N., Nedoluha, G. E., Gomez, R. M., Eriksson, P., Forkman, P., Lambert, A., and Schwartz, M. J.: Validation of ground-based microwave radiometers at 22 GHz for stratospheric and mesospheric water vapor, J. Geophys. Res., 114, D23305, doi:10.1029/2009JD011997, 2009.

Hoogen, R., Rozanov, V. V., and Burrows, J. P.: Ozone profiles from GOME satellite data: description and first validation Algorithm, J. Geophys. Res., 104(D7), 8263–8280, 1999.

Janssen, M. A.: Atmospheric Remote Sensing by Microwave radiometry, John Wiley & Sons, Inc., New York, 1993.

Kraus, J. D.: Radio Astronomy, McGraw-Hill, New York, 1966.

Kuntz, M., Kopp, G., Berg, H., Hochschilda, G., and Krupa, R.: Joint retrieval of atmospheric constituent profiles from ground-based millimetre-wave measurements: ClO, HNO$_3$, N$_2$O, and O$_3$, J. Geophys Res. 104(D11), 13981–13992, 1999.

Livesey N. J., Read, W. G., Froidevaux, L., Waters, J. W., Santee, M. L., Pumphrey, H. C., Wu, D. L., Shippony, Z., and Jarnot, R. F.: The UARS Microwave Limb Sounder version 5 data set: theory, characterization, and validation, J. Geophys. Res., 108(D13), 4378, doi:10.1029/2002JD002273, 2003.

McDonald, M., de Zafra, R. L., and Muscari, G.: Millimeter wave spectroscopic measurements over the South Pole: 5. Morphology and evolution of HNO$_3$ vertical distribution, 1993 versus 1995, J. Geophys. Res., 105(D14), 17739–17750, 2000.

Muscari, G., Santee, M. L., and de Zafra, R. L.: Intercomparison of stratospheric HNO$_3$ measurements over Antarctica: Ground-based millimeter-wave versus UARS/MLS version 5 retrievals, J. Geophys. Res., 107(D24), 4809, doi:10.1029/2002JD002546, 2002.

Muscari, G., de Zafra, R. L., and Smyshlyaev, S.: Evolution of the NO$_y$-N$_2$O correlation in the Antarctic stratosphere during 1993 and 1995, J. Geophys. Res., 108(D14), 4428, doi:10.1029/2002JD002871, 2003.

Muscari, G., di Sarra, A. G., de Zafra, R. L., Lucci, F., Baordo, F., Angelini, F., and Fiocco, G.: Middle atmospheric O$_3$, CO, N$_2$O, HNO$_3$, and temperature profiles during the warm Arctic winter 2001–2002, J. Geophys. Res., 112, D14304,

doi:10.1029/2006JD007849, 2007.

Nagahama, T., Nakane, H., Fujinuma, Y., Ninomiya, M., Ogawa, H., and Fukui, Y.: Ground-based millimeter-wave observations of ozone in the upper stratosphere and mesosphere over Tsukuba, Earth Planets Space, 51, 1287–1296, 1999.

Nedoluha, G., Bevilacqua, R., Gomez, R., Thacker, D., Waltman, W., and Pauls, T.: Ground-based measurements of water vapor in the middle atmosphere, J. Geophys. Res., 100(D2), 2927–2939, 1995.

Newman, P. A., Nash, E. R., Kawa, S. R., Montzka, S. A., and Schauffler, S. M.: When will the Antarctic ozone hole recover?, Geophys. Res. Lett., 33, L12814, doi:10.1029/2005GL025232, 2006.

Parrish, A., de Zafra, R. L., Solomon, P. M., and Barrett, J. W.: A ground-based technique for millimeter wave spectroscopic observations of stratospheric trace constituents, Radio Sci., 23, 106–118, 1988.

Parrish, A., Connor, B. J., Tsou, J. J., Mc Dermid, I. S., and Chu, W. P.: Ground-Based Microwave Monitoring of Stratospheric Ozone, J. Geophys. Res., 97(D2), 2541–2546, 1992.

Petkie, D. T., Helminger, P. A, Butler, R. A., Albert, S., and De Lucia, F. C.: The millimeter and submillimeter spectra of the ground and exited ν_9, ν_8, ν_7 and ν_6 vibrational states of HNO$_3$, J. Mol. Spectrosc., 218, 127–130, 2003.

Rodgers, C. D.: Retrieval of atmospheric temperature and composition from remote measurements of thermal radiation, Rev. Geophys. Space Ge., 14(4), 609–624, 1976.

Rodgers, C. D.: Inverse method for atmospheric sounding, Series on atmospheric, oceanic and Planetary Physics – vol.2, Taylor, F. W., World Scientific Publishing Co. Pte LTd, Singapore, 2000.

Rothman, L. S., Gordon, I. E., Barbe, A., Chris Benner, D., Bernath, P. F., Birk, M., Boudon, V., Brown, L. R., Campargue, A., Champion, J. P., Chance, K., Coudert, L. H., Dana, V., Devi, V. M., Fally, S., Flaud, J. M., Gamache, R. R., Goldman, A., Jacquemart, D., Kleiner, I., Lacome, N., Lafferty, W. J., Mandin, J. Y., Massie, S. T., Mikhailenko, S. N., Miller, C. E., Moazzen-Ahmadi, N., Naumenko, O. V., Nikitin, A. V., Orphal, J., Perevalov, V. I., Perrin, A., Predoi-Cross, A., Rinsland, C. P., Rotger, M., Simeckova, M., Smith, M. A. H., Sung, K., Tashkun, S. A., Tennyson, J., Toth, R. A., Vandaele, A. C., and Vander Auwera, J.: The HITRAN 2008 molecular spectroscopic database, J. Quant. Spectrosc. Ra., 110, 533–572, 2009.

Santee, M., Lambert, A., Read, W., Livesey, N., Coeld, R., Cuddy, D., Daffer, W., Drouin, B., Froidevaux, L., Fuller, R., Jarnot, R., Knosp, B., Manney, G., Perun, V., Snyder, W., Stek, P., Thurstans, R., Wagner, P., Waters, J., Muscari, G., de Zafra, R., Dibb, J., Fahey, D., Popp, P., Marcy, T., Jucks K., Toon, G., Stachnik, R., Bernath, P., Boone, C., Walker, K., Urban, J., and Murtagh, D.: Validation of the Aura Microwave Limb Sounder HNO$_3$ Measurements, J. Geophys. Res., 112, D24S40, doi:10.1029/2007JD008721, 2007.

Solomon, S., Garcia, R. R., Rowland, F. S., and Wuebbles, D. J.: On the depletion of Antarctic ozone, Nature, 321, 755–758, 1986.

Tabazadeh, A., Santee, M. L., Danlin, M. Y., Pumphrey, H. C., Newman, P. A., Hamill, P. J., and Mergenthaler, J. L.: Quantifying Denitrification and Its Effect on Ozone Recovery, Science, 288(5470), 1407–1411, 2000.

Tabazadeh, A., Jensen, E. J., Toon, O. B., Drdla, K., and Schoeberl, M. R.: Role of the Stratospheric Polar Freezing Belt in Denitrifi-

cation, Science, 291(5513), 2591–2594, 2001.

Twomey, S.: Introduction to the Mathematics of Inversion in Remote Sensing and Indirect Measurements, Developments in Geomathematics, 3, Elsevier Sci., New York, 1977.

Waters, J. W., Froidevaux, L., Harwood, R. S., Jarnot, R. F., Pickett, H. M., Read, W. G., Siegel, P. H., Cofield, R. E., Filipiak, M. J., Flower, D. A., Holden, J. R., Lau, G. K., Livesey, N. J., Manney, G. L., Pumphrey, H. C., Santee, M. L., Wu, D. L., Cuddy, D. T., Lay, R. R., Loo, M. S., Vincent, S. Perun, V. S., Schwartz, M. J., Stek, P. C., Thurstans, R. P., Boyles, M. A., Chandra, K. M., Chavez, M. C., Chen, G. S., Chudasama, B. V., Dodge, R., Fuller, R. A., Girard, M. A., Jiang, J. H., Jiang, Y., Knosp, B. W., LaBelle, R. C., Lam, J. C., Lee, K. A., Miller, D., Oswald, J. E., Patel, N. C., Pukala, D. M., Quintero, O., Scaff, D. M., Van Snyder, W., Tope, M. C., Wagner, P. A., and Walch, M. J.: The Earth Observing System Microwave Limb Sounder (EOS MLS) on the Aura satellite, IEEE T. Geosci. Remote, 44, 5, doi:10.1109/TGRS.2006.873771, 2006.

WMO (World Meteorological Organization): Scientific Assessment of Ozone Depletion: 2006, Global Ozone Research and Monitoring Project – Report No. 50, 572 pp., Geneva, Switzerland, 2007.